

# Penetration depth, multiband superconductivity, and absence of muon-induced perturbation in superconducting $\text{PrOs}_4\text{Sb}_{12}$

Lei Shu\*, D. E. MacLaughlin, and W. P. Beyermann  
*Department of Physics, University of California, Riverside, California 92521*

R. H. Heffner  
*Los Alamos National Laboratory, Los Alamos, New Mexico 87545*

G. D. Morris  
*TRIUMF, 4004 Wesbrook Mall, Vancouver, B.C., Canada V6T 2A3*

O. O. Bernal  
*Department of Physics and Astronomy, California State University, Los Angeles, California 90032*

F. D. Callaghan and J. E. Sonier  
*Department of Physics, Simon Fraser University, Burnaby, B.C., Canada V5A 1S6*

W. M. Yuhasz, N. A. Frederick, and M. B. Maple  
*Department of Physics and Institute for Pure and Applied Physical Sciences,  
University of California, San Diego, La Jolla, California 92093*  
(Dated: November 10, 2019)

Transverse-field muon spin rotation ( $\mu\text{SR}$ ) experiments in the heavy-fermion superconductor  $\text{PrOs}_4\text{Sb}_{12}$  ( $T_c = 1.85$  K) suggest that the superconducting penetration depth  $\lambda(T)$  is temperature-independent at low temperatures, consistent with a gapped quasiparticle excitation spectrum. In contrast, radiofrequency (rf) inductive measurements yield a stronger temperature dependence of  $\lambda(T)$ , indicative of point nodes in the gap. This discrepancy appears to be related to the multiband structure of  $\text{PrOs}_4\text{Sb}_{12}$ . Muon Knight shift measurements in  $\text{PrOs}_4\text{Sb}_{12}$  suggest that the perturbing effect of the muon charge on the neighboring  $\text{Pr}^{3+}$  crystalline electric field is negligibly small, and therefore is unlikely to cause the difference between the  $\mu\text{SR}$  and rf results.

PACS numbers: 71.27.+a, 71.70.Ch, 74.70.Tx, 75.10.Dg, 76.75.+i

## I. INTRODUCTION

In the phenomenon of multiband superconductivity (MBSC), which was first treated theoretically in 1959 using BCS theory,<sup>1</sup> distinct energy gaps open up on different sheets of the Fermi surface in the superconducting state. One of the well-studied multiband superconductors is the binary intermetallic compound  $\text{MgB}_2$ ,<sup>2,3,4</sup> which has two bands and two superconducting gaps. Based on a quasiclassical theory, microscopic calculations of the electronic structure in the vortex state have been made in a two-band superconducting model.<sup>5,6</sup> These suggest that at low applied fields the dominant contribution to the change of the total density of states (DOS) comes from the small-gap band, which gives rise to spatially extended quasiparticles (QPs). At high fields these loosely bound states become delocalized, with the vortex core size determined by the more localized states associated with the larger gap. The presence of delocalized

QPs will modify the DOS, transport properties associated with the quasiparticles, and spatial field distribution around the vortex.<sup>7</sup>

Recently strong evidence for MBSC has been found in the filled skutterudite  $\text{PrOs}_4\text{Sb}_{12}$  from thermal transport measurements in the vortex state.<sup>8,9</sup>  $\text{PrOs}_4\text{Sb}_{12}$  has attracted much attention since it was discovered in 2002.<sup>10</sup> It is the only known Pr-based heavy-fermion superconductor ( $T_c = 1.85$  K, Ref. 10) and exhibits a number of extraordinary properties.<sup>11</sup> The  $\text{Pr}^{3+}$  ground state is nonmagnetic  $\Gamma_1$  singlet, which is separated from a  $\Gamma_4^{(2)}$  first excited state (tetrahedral notation<sup>12</sup>) by only  $\sim 10$  K,<sup>13,14,15,16</sup> and a novel ordered phase appears at high fields and low temperatures. There is evidence that time-reversal symmetry is broken in the superconducting state.<sup>17</sup> Radiofrequency (rf) inductive measurements of the surface penetration depth,<sup>18</sup> thermal conductivity measurements in a rotated magnetic field,<sup>19</sup> and flux-line lattice distortion<sup>20</sup> all suggest nodes in the superconducting gap. A double superconducting transition has been observed in the specific heat measurements.<sup>13,21,22,23</sup> However, a very recent heat transport measurement<sup>9</sup> on a highly homogeneous single crystal shows only one transition peak in the specific heat and a fully open gap. Our previous  $\mu\text{SR}$  measurements of

---

\*Current address: Department of Physics and Institute for Pure and Applied Physical Sciences, University of California, San Diego, La Jolla, California 92093

the magnetic penetration depth  $\lambda$  in the vortex state of a powdered sample<sup>24</sup> found evidence for a BCS-like activated dependence at low temperature, suggesting the absence of gap nodes. Thus there are a number of open questions about the superconducting order parameter in this compound.

Transverse-field muon spin rotation (TF- $\mu$ SR)<sup>25</sup> experiments have proved invaluable in characterizing both the superconducting and normal state.<sup>26</sup> This article reports new TF- $\mu$ SR experiments on oriented PrOs<sub>4</sub>Sb<sub>12</sub> crystals. We compare  $\mu$ SR and surface penetration depth measurements in PrOs<sub>4</sub>Sb<sub>12</sub>, and find a discrepancy between the results of these measurements that can be understood as a consequence of MBSC in PrOs<sub>4</sub>Sb<sub>12</sub>. Previous results<sup>27</sup> and preliminary report of this work have been published.<sup>28</sup> Furthermore, TF- $\mu$ SR measurements of the Knight shift in the normal state of PrOs<sub>4</sub>Sb<sub>12</sub> suggest that the perturbing effect of the  $\mu^+$  charge on the neighboring Pr<sup>3+</sup> crystalline electric fields (CEF) is negligibly small. This indicates that the muon charge is unlikely to be the source of the discrepancy. A model calculation for the perturbed CEF energy levels, based on the approach of Kaplan, Schenck, and co-workers,<sup>29,30,31,32</sup> is described.

The remainder of this introduction contains three brief pedagogical sections: a description of the elements of the TF- $\mu$ SR technique used in this study (Sec. IA), a review of the important features of the muon Knight shift (Sec. IB), and an introduction to the CEF model calculation (Sec. IC). After a description of the experimental procedure (Sec. II), in Sec. III we describe our experimental results in PrOs<sub>4</sub>Sb<sub>12</sub>, which include the temperature dependence of the TF- $\mu$ SR relaxation rate and penetration depth, magnetic susceptibility data, and normal-state  $\mu^+$  Knight shift measurements. The implications of these results for the nature of both the superconducting and the normal state are discussed in Sec. IV. We summarize our results in Sec. V.

### A. Transverse-field muon spin rotation

In the TF- $\mu$ SR technique<sup>25</sup> spin-polarized positive muons ( $\mu^+$ ) are implanted in the sample and precess in a local magnetic field applied perpendicular to the  $\mu^+$  spin. This precession is detected using the asymmetry of the  $\mu^+$  beta decay (the decay positron is emitted preferentially in the direction of the  $\mu^+$  spin). The distribution of  $\mu^+$  precession frequencies directly reflects the distribution of magnetic fields in the sample. Thus TF- $\mu$ SR can be used to measure the magnetic field distribution of the vortex lattice in a type-II superconductor and the local magnetic susceptibility in the normal state.

In the vortex lattice each vortex possesses a normal-state-like core with radius of order of the superconducting coherence length  $\xi$ , surrounded by a shielding supercurrent. These supercurrents give rise to an inhomogeneous magnetic field that is periodic in the vortex lattice. TF-

$\mu$ SR experiments are sensitive probes of this field distribution.<sup>26</sup> The exact functional form of the muon spin relaxation, which depends on the field distribution, can be fitted with the functional form  $G(t) \cos(\omega t + \phi)$ , where the frequency  $\omega$  and phase  $\phi$  describe the average  $\mu^+$  precession and the relaxation function  $G(t)$  describes the loss of phase coherence due to the distribution of precession frequencies. The relaxation rate associated with  $G(t)$  is a measure of the rms width  $\delta B$  of this distribution. The expression<sup>33</sup>

$$\delta B^2(T) = 0.00371 \Phi_0^2 \lambda^{-4}(T), \quad (1)$$

where  $\Phi_0$  is the flux quantum, relates the second moment  $\delta B^2$  of field distribution to the magnetic penetration depth  $\lambda$  for a triangular vortex lattice in the London limit ( $\lambda \gg \xi$ ).

To estimate the field distribution one often assumes a Gaussian distribution of local fields. Then the time dependence of the muon spin polarization is proportional to  $\exp(-\frac{1}{2}\sigma^2 t^2)$ , where  $\sigma = \gamma_\mu \delta B$  is the muon relaxation rate and  $\gamma_\mu$  is the muon gyromagnetic ratio. However, it has been pointed out that this approximation can be inaccurate if there are other sizeable contributions to the  $\mu$ SR linewidth that vary in a manner different from  $\lambda$ .<sup>26</sup> An analytical Ginzburg-Landau (GL) model for the spatial field profile has therefore been proposed. The  $\mu$ SR time spectra can be fit to the GL model for the spatial field profile of the vortex lattice for  $H \ll H_{c2}$  (Refs. 26 and 34):

$$\mathbf{B}(\mathbf{r}) = B_0(1 - b^4) \sum_{\mathbf{K}} \frac{e^{-i\mathbf{K}\cdot\mathbf{r}} u K_1(u)}{\lambda^2 K^2} \hat{\mathbf{z}}, \quad (2)$$

where the  $\mathbf{K}$  are the reciprocal-lattice vectors of the unit cell,  $K_1(u)$  is a modified Bessel function,  $b = B/B_{c2}$  is the reduced field, and

$$u^2 = 2\xi^2 K^2(1 + b^4)[1 - 2b(1 - b)^2], \quad (3)$$

with  $\xi$  the GL coherence length. The exact form of the muon spin relaxation function is the Fourier transform of the magnetic-field distribution function, which can be obtained from Eq. (2). A lineshape analysis program has been written<sup>26</sup> to fit this GL model to the data; results from such fits in PrOs<sub>4</sub>Sb<sub>12</sub> are described below in Sec. III A.

### B. Muon Knight shift

In TF- $\mu$ SR, when an external field is applied perpendicular to the initial  $\mu^+$  polarization, the total field at the  $\mu^+$  site is given by the sum of applied field, the internal fields induced by the applied field, and the demagnetization and Lorentz fields.<sup>35</sup> The relative  $\mu^+$  frequency shift

$$K_\mu^* = \frac{\omega_\mu}{\omega_{\text{ref}}} - 1, \quad (4)$$

where  $\omega_{\text{ref}} = \gamma_{\mu} H_{\text{ref}}$  is the  $\mu^+$  frequency in “free space” (i.e., no condensed matter effects), must be corrected for the contribution of the demagnetization and Lorentz fields  $K_{\text{DL}}$  to obtain the  $\mu^+$  Knight shift<sup>36</sup>

$$K_{\mu} = K_{\mu}^* - K_{\text{DL}}, \quad (5)$$

which contains the relevant information about the hyperfine fields.

In a paramagnetic metal,  $K_{\mu}$  originates from hyperfine fields produced by the polarization of conduction electrons and localized electronic moments induced by the external field. The contribution from the conduction electrons is temperature independent and is usually very small, of the order of 100 ppm.<sup>36</sup> The localized electrons, in the present work the  $4f$  electrons of the  $\text{Pr}^{3+}$  ions, contribute to  $K_{\mu}$  via two mechanisms. The first is the dipole-dipole interaction between the local moments and the  $\mu^+$ , which may be described as a dipolar field at the  $\mu^+$  interstitial site. The second contribution to  $K_{\mu}$  arises from the indirect RKKY interaction,<sup>36</sup> in which an additional spin polarization of the conduction electrons due to the  $f$  localized moments produces hyperfine contact field at the interstitial  $\mu^+$ . Both contributions are proportional to the  $f$  paramagnetic susceptibility:

$$K_{\mu}^i = (A_{\text{dip}}^{ii} + A_{\text{con}}) \chi_i \quad (i = x, y, z), \quad (6)$$

where  $A_{\text{dip}}^{ii}$  and  $A_{\text{con}}$  are the dipolar and hyperfine coupling constants respectively (the  $A^{ii}$  are the on-diagonal elements of the dipolar coupling tensor). For a cubic lattice, only the hyperfine contact field at the interstitial  $\mu^+$  site contributes to the average shift  $K_{\mu} = \frac{1}{3} \sum_i K_{\mu}^i$ , since the contribution from the dipole-dipole interaction vanishes.

The local  $f$  susceptibility is sensitive to change in the  $f$ -ion CEF, and the  $\mu^+$  charge may induce such a change. If so, the modified local susceptibility will be reflected in a breakdown of the proportionality of the  $\mu^+$  Knight shift to the measured bulk susceptibility  $\chi^{\text{bulk}}$  since in this case  $\chi_i \neq \chi^{\text{bulk}}$ . This effect has been studied in detail by Kaplan, Schenck, and co-workers<sup>29,30,31,32</sup> in Pr-based compounds with singlet  $\text{Pr}^{3+}$  CEF ground states. As noted above and discussed in Sec. IV B, our results in  $\text{PrOs}_4\text{Sb}_{12}$  show little if any such effect.

### C. CEF model calculation

The crystal structure of  $\text{PrOs}_4\text{Sb}_{12}$  belongs to the  $Im\bar{3}$  space group, with  $\text{Pr}^{3+}$  ions at the points of a bcc unit cell. As approximation we may assume the CEF Hamiltonian  $\mathcal{H}_{\text{CEF}}$  for the  $\text{Pr}^{3+}$  ions has cubic  $O_h$  point group symmetry. Then

$$\mathcal{H}_{\text{CEF}} = B_4^0 O_4^0 + 5B_4^0 O_4^4 + B_6^0 O_6^0 - 21B_6^0 O_6^4, \quad (7)$$

where  $O_4^0$ ,  $O_4^4$ ,  $O_6^0$ , and  $O_6^4$  are the Stevens operators for a given  $J$ <sup>37</sup> and the  $B$ s are parameters determined from

the experiment, splits the  $J = 4$  Hund’s rule multiplet of  $\text{Pr}^{3+}$  into a singlet ( $\Gamma_1$ ), a doublet ( $\Gamma_3$ ), and two triplets ( $\Gamma_4$  and  $\Gamma_5$ ). The actual symmetry of the  $\text{Pr}^{3+}$  ions in  $\text{PrOs}_4\text{Sb}_{12}$  is, however, that of the tetrahedral  $T_h$  point group,<sup>12</sup> for which an additional sixth-order term appears in the CEF Hamiltonian [Eq. (7)]. This term mixes the  $\Gamma_4$  and  $\Gamma_5$  triplet wave functions with each other,<sup>12</sup> but has a relatively small effect on the CEF energies.<sup>16</sup> If it is predominant, a  $\Gamma_4$  or  $\Gamma_5$  triplet will be the ground state, inconsistent with the ground state in nonmagnetic  $\text{PrOs}_4\text{Sb}_{12}$ . However, if this term is small, the change in the physical properties in zero magnetic field can be approximated by changing the parameters in the cubic CEF Hamiltonian [Eq. (7)] slightly. Thus we use the cubic CEF Hamiltonian for simplicity.

In the presence of an external magnetic field, the Zeeman interaction mixes and splits the CEF energy levels. The magnetic susceptibility is given by<sup>32</sup>

$$\chi_{\text{CEF}} = \frac{\sum_n \left[ (E_n^{(1)})^2 / kT - 2E_n^{(2)} \right] \exp \left( -E_n^{(0)} / kT \right)}{\sum_n \exp \left( -E_n^{(0)} / kT \right)}, \quad (8)$$

where the  $E_n^{(0)}$  are the unperturbed cubic CEF levels,  $E_n^{(1)} = \mu_B g \langle \phi_n | J | \phi_n \rangle$  with  $\phi$  the CEF wave functions and  $g$  the Landé  $g$ -factor, and

$$E_n^{(2)} = \sum_{n' \neq n} \mu_B^2 g^2 \frac{|\langle \phi_n | J | \phi_{n'} \rangle|^2}{E_n^{(0)} - E_{n'}^{(0)}}. \quad (9)$$

In the molecular-field approximation, the measured magnetic susceptibility  $\chi$  is given by  $\chi = \chi_{\text{CEF}} / (1 - \ell \chi_{\text{CEF}})$ , where  $\ell$  is the molecular field parameter that describes exchange interactions between  $\text{Pr}^{3+}$  ions.<sup>38</sup>

Equation (8) shows that the observed  $\chi$  is directly related to the local CEF energy levels. As noted above, if we take into account possible muon-induced change of the CEF, we must consider a modified CEF Hamiltonian to calculate the resultant change of the  $\text{Pr}^{3+}$  local susceptibility.<sup>29,30,31,32</sup> In  $\text{PrOs}_4\text{Sb}_{12}$  the  $\text{Pr}^{3+}$  first excited state is separated from the singlet ground state by only  $\sim 10$  K.<sup>13,14,15,16</sup> Hence it is important to determine possible changes in the local CEF energy levels by the  $\mu^+$  charge particularly, since such changes might affect other local properties such as the vortex-state field distribution.

## II. EXPERIMENTS

TF- $\mu$ SR experiments were carried out at the M15 and M20 channels at TRIUMF, Vancouver, Canada, on a mosaic of oriented  $\text{PrOs}_4\text{Sb}_{12}$  crystals. The crystals were mounted on a thin GaAs backing, which rapidly depolarizes muons in transverse field and minimizes any spurious signal from muons that do not stop in the sample.  $\mu$ SR asymmetry data<sup>26</sup> were taken for temperatures in the range 0.02–250 K and  $\mu_0 H$  between 10 mT and 1.0

T applied parallel to the  $\langle 100 \rangle$  axes of the crystals. For the muon Knight shift measurements, the applied field was determined by measuring the precession frequency of muons that stopped in a small piece of silver foil included with the sample.

### III. EXPERIMENTAL RESULTS

#### A. Transverse-field muon spin relaxation and magnetic penetration depth

As a first step, transverse-field muon spin relaxation functions were fitted with the functional form  $G(t) \cos(\omega t + \phi)$ . Data from both the normal and superconducting states could be fit by the damped Gaussian

$$G(t) = e^{-Wt} \exp(-\frac{1}{2}\sigma^2 t^2). \quad (10)$$

Below  $T_c$  the exponential rate  $W$  was fixed at the normal-state value for each field, so that the temperature dependence of the Gaussian rate  $\sigma$  reflects the effect of the superconducting state. Some such procedure is necessitated by the strong statistical correlation between  $W$  and  $\sigma$  in Eq. 10; the time constant and the shape of the function are influenced by both of these parameters, so that correlations between them can result from small systematic errors. The principal justification for this *ad hoc* fixing of  $W$  is the insensitivity of the superconducting-state results to details of the fitting function [Eq. (10)] discussed below. Determination of the vortex-state field distribution width requires correction for the normal-state relaxation. We take the superconducting-state Gaussian rate  $\sigma_s$  to be given by  $\sigma_s^2 = \sigma^2 - \sigma_n^2$ , where  $\sigma_n$  is the normal-state rate.<sup>26</sup>

Figure 1 gives the temperature dependence of the corrected superconducting-state  $\mu^+$  relaxation rates  $\sigma_s$  for  $\mu_0 H = 10, 20,$  and  $100$  mT. At 10 and 20 mT  $\sigma_s$  is nearly temperature-independent below  $\sim 0.8$  K. At the lowest temperatures the rate is field-independent to within a few percent between 10 mT and 100 mT. In an isotropic superconductor such as cubic  $\text{PrOs}_4\text{Sb}_{12}$  vortex-lattice disorder is expected to increase the low-field rate; increasing field (increasing vortex density) then decreases the rate as intervortex interactions stabilize the lattice.<sup>26,39</sup> Thus the field independence of the rate indicates a substantially ordered vortex lattice, in which case the temperature dependence of the rate is controlled solely by the temperature dependence of the field distribution.

Equation (1) relates the second moment  $\delta B^2$  of field distribution to  $\lambda$  in the London limit. The second moment of the corresponding  $\mu^+$  frequency distribution is  $\delta\omega^2 = \gamma_\mu^2 \delta B^2$ , where  $\gamma_\mu$  is the  $\mu^+$  gyromagnetic ratio. Then the estimated penetration depth  $\lambda$  from Eq. (1) is

$$\lambda(\mu\text{m}) = 0.328 / \sqrt{\delta\omega(\mu\text{s}^{-1})}. \quad (11)$$

Now the rms width  $\sigma_s$  of the best-fit Gaussian is not necessarily  $\delta\omega$ , and replacement of  $\delta\omega$  in Eq. (11) by  $\sigma_s$

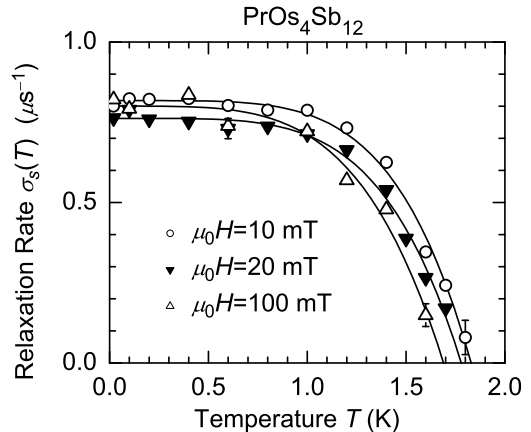


FIG. 1: Temperature dependence of superconducting-state relaxation rates in  $\text{PrOs}_4\text{Sb}_{12}$ , corrected for normal-state relaxation (see text).

is not completely justified. Nevertheless  $\sigma_s$  should scale with  $\delta\omega$ , and within its range of validity Eq. (11) should give the correct temperature dependence of  $\lambda$ . This is because under these circumstances effects of nonzero  $\xi$  are restricted to the high-field tail of field distribution, which is not heavily weighted in a Gaussian fit (cf. Fig. 1 of Ref. 40).  $\text{PrOs}_4\text{Sb}_{12}$  is a strongly type-II superconductor (GL  $\kappa = \lambda/\xi \approx 30$ , Ref. 10 and 24), and this picture should be applicable.

The temperature dependence of  $\lambda$  obtained from Eq. (11) is shown in the inset of Fig. 2 (circles) for an applied field of 10 mT. It can be seen that  $\lambda(T)$  is constant below  $\sim 1$  K, indicative of a gapped quasiparticle excitation spectrum.

To verify this conclusion, the GL model was also fit to our  $\mu\text{SR}$  data as described in Sec. IA. The values of  $\lambda$  from these fits, also shown in the inset of Fig. 2 (squares), agree very well with those from Gaussian fits. The BCS low-temperature expression  $\lambda(T) = \lambda(0)(1 + \sqrt{\frac{\pi\Delta}{2T}} e^{-\Delta/T})$  (Ref. 24, curve in Fig. 2) gives a good fit to the data for  $T \leq 0.5T_c$ , suggesting that the energy gap is isotropic. However, rf measurements of the surface penetration depth in the Meissner state<sup>18</sup> suggest point nodes in the energy gap. We have compared  $\lambda_{\text{rf}}(T) = \Delta\lambda_{\text{rf}}(T) + \lambda(0)$ , obtained from these measurements,<sup>18</sup> with  $\lambda_{\mu\text{SR}}(T)$ , obtained using the  $\mu^+$  data for  $\mu_0 H = 10$  mT.<sup>34</sup> At low temperatures the increase of  $\lambda_{\text{rf}}(T)$  with increasing temperature is much stronger than the increasing of  $\lambda_{\mu\text{SR}}(T)$ ; this is the discrepancy between the measurements noted above. A possible resolution of this discrepancy is discussed in Sec. IV A.

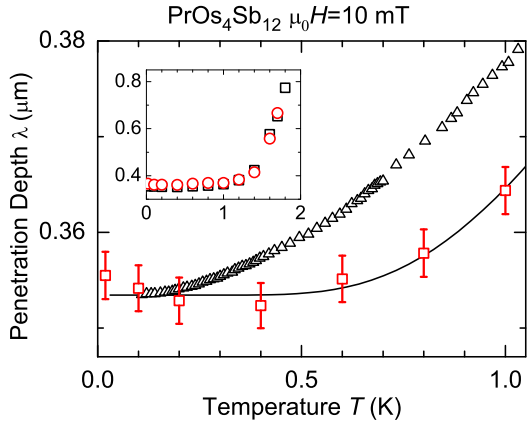


FIG. 2: Low temperature dependence of penetration depth  $\lambda$  in  $\text{PrOs}_4\text{Sb}_{12}$ . Triangles: rf measurements of the surface penetration depth in the Meissner state<sup>18</sup>. Squares:  $\lambda$  from GL model fitting. Curve:  $\lambda(T) = \lambda(0)[1 + \sqrt{\frac{\pi\Delta}{2T}} e^{-\Delta/T}]$ ,  $\lambda(0) = 0.3534(24) \mu\text{m}$ ,  $2\Delta/k_B T_c = 4.9(1)$ . Inset: Temperature dependence of  $\lambda$  up to  $T_c$ . Circles:  $\lambda$  from Gaussian fit.

### B. Magnetic susceptibility

The temperature dependence of the normal-state magnetic susceptibility of the  $\text{PrOs}_4\text{Sb}_{12}$ , sample used in the  $\mu\text{SR}$  experiments has been determined using a commercial SQUID magnetometer. Figure 3 shows the measured bulk susceptibility (circles). The data were fit to the model of CEF-split  $\text{Pr}^{3+}$  ions with cubic  $O_h$  symmetry interacting via a molecular field as discussed in Sec. IC. The resulting temperature dependence is given by the curve in Fig. 3. The fit values of the CEF parameters in Eq. (7) are listed in Table I. The fit value of the molecular field parameter  $\ell$  was found to be  $-1.67$  mole/emu, which is close to the value of  $-2.54$  mole/emu found by Tayama *et al.*<sup>41</sup>

### C. Muon Knight shift

We have performed TF- $\mu\text{SR}$  experiments at applied field  $\mu_0 H = 1.0$  T in the normal state of  $\text{PrOs}_4\text{Sb}_{12}$  to measure the muon Knight shift. Since the frequency shift is proportional to the magnetic field at the muon site, higher fields help to resolve the shift. Fig. 4(a) shows the temperature dependence of the muon-spin precession frequencies from the sample and an Ag reference. Silver was used because Ag nuclear dipole fields are weak, and the  $\mu^+$  Knight shift in Ag is known (94 ppm).<sup>42</sup> One can extract the  $\mu^+$  frequency to an accuracy of  $\sim 100$  ppm.<sup>29</sup> The temperature dependence of the relative  $\mu^+$  frequency shift  $K_\mu^*$  is shown in Fig. 4 (b).

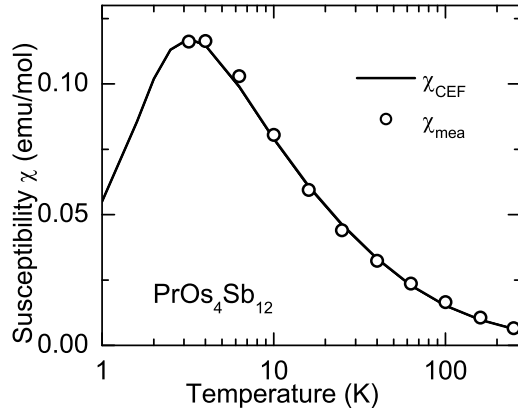


FIG. 3: Temperature dependence of measured bulk susceptibility (circles) and best fit to model of interacting CEF-split  $\text{Pr}^{3+}$  ions (curve) in  $\text{PrOs}_4\text{Sb}_{12}$ .

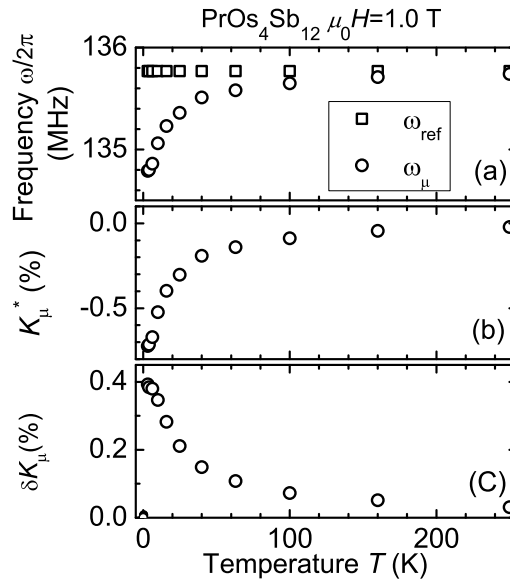


FIG. 4: (a): Temperature dependencies of  $\mu^+$  precession frequencies in  $\text{PrOs}_4\text{Sb}_{12}$  ( $\omega_\mu$ ) and an Ag reference ( $\omega_{\text{ref}}$ ). (b): Temperature dependence of  $\mu^+$  frequency shift  $K_\mu^*$  in the normal state. (c): Temperature dependence of relative rms linewidth  $\delta K_\mu = \sigma/\omega_{\text{ref}}$ , where  $\sigma$  is the  $\mu^+$  Gaussian relaxation rate.

TABLE I: Fit values of CEF parameters in meV for  $\text{PrOs}_4\text{Sb}_{12}$ .  $O_h$ : cubic symmetry (no  $\mu^+$  perturbation).  $C_{4v}$ : tetragonal symmetry ( $\mu^+$  perturbation, cf. Sec. IV B).

$B_2^0$		$B_4^0$		$B_4^4$		$B_6^0$		$B_6^4$	
$O_h$	$C_{4v}$	$O_h$	$C_{4v}$	$O_h$	$C_{4v}$	$O_h$	$C_{4v}$	$O_h$	$C_{4v}$
0	0.04	0.0154	0.0153	0.0771	0.0771	0.0007	0.0007	-0.0154	-0.0154

Figure 5 (triangles) gives the dependence of  $K_\mu^*$  on the bulk molar susceptibility  $\chi_{\text{mol}}^{\text{bulk}}$  in  $\text{PrOs}_4\text{Sb}_{12}$  in the normal state, with temperature an implicit variable.  $K_\mu^*$  and  $\chi_{\text{mol}}^{\text{bulk}}$  were measured in the same sample. As discussed in Sect. IB,  $K_\mu^*$  should be corrected for the effect of the Lorentz and demagnetization fields  $4\pi(1/3 - n)M$ , where  $M$  is the magnetization. The demagnetization factor  $n$  was estimated from (i) the ratio of the height and width of the samples,<sup>43</sup> with the magnetic field applied perpendicular to the flat faces of the rectangular crystallites, and (ii) the ratio  $f$  of individual crystal volume to the sample as a whole, taking spaces between the crystallites into account. We estimate the demagnetization factor for the entire sample  $n_{\text{sam}} = 0.824$ , the demagnetization factor for individual crystals  $n_{\text{cryst}} = 0.365$ ,<sup>43</sup> and  $f = 0.95$ . Then the effective value is  $n = fn_{\text{sam}} + (1 - f)n_{\text{cryst}} = 0.80$ .<sup>44</sup> Therefore,  $K_{\text{DL}} = 4\pi(1/3 - n)\chi_V^{\text{bulk}} = -4\pi(0.47)\chi_V^{\text{bulk}}$ , where  $\chi_V^{\text{bulk}}$  is the bulk susceptibility per unit volume, or  $K_{\text{DL}} = -0.0243\chi_{\text{mol}}^{\text{bulk}}$ . We subtract this from  $K_\mu^*$  to obtain the corrected  $\mu^+$  Knight shift  $K_\mu$  (Fig. 5, circles). A linear relation is obtained for  $\chi_{\text{mol}}^{\text{bulk}} \lesssim 8.0 \times 10^{-2}$

from the “bulk” Knight shift  $K_{\text{bulk}}$  in the absence of local perturbations. Only a small deviation from linearity appears below 6.3 K.

As discussed in Sec. IB, the average shift arises solely from the hyperfine contact field at the interstitial  $\mu^+$  for a cubic lattice. The dipole-dipole interaction, however, may split or broaden the  $\mu^+$  line. Assuming the most probable  $\mu^+$  stopping site  $(\frac{1}{2}, 0, 0.15)$  determined by Aoki *et al.*,<sup>17</sup> and supposing only the dipolar field contributes to the Knight shift anisotropy, we obtain an anisotropic Knight shift tensor with the following principal values for field directions  $(x, y, z)$ :  $K_{\text{dip}}^x = 4.64 \times 10^{-2}\chi_{\text{mol}}$ ,  $K_{\text{dip}}^y = -2.51 \times 10^{-2}\chi_{\text{mol}}$ , and  $K_{\text{dip}}^z = -2.01 \times 10^{-2}\chi_{\text{mol}}$ . Thus the  $\mu^+$  resonance should be split into three lines of equal weight. The observed relative rms linewidth  $\delta K_\mu = 4.68 \times 10^{-2}\chi_{\text{mol}}$  (data not shown) is, however, somewhat larger than the rms spread  $\Delta K_{\text{dip}} = \sqrt{[(K_{\text{dip}}^x)^2 + (K_{\text{dip}}^y)^2 + (K_{\text{dip}}^z)^2]/3} = 3.26 \times 10^{-2}\chi_{\text{mol}}$ . Thus the dipolar splitting cannot be resolved, although it contributes significantly to the linewidth.

## IV. DISCUSSION

### A. Multiband Superconductivity

We first consider the discrepancy in measured magnetic penetration depth between the  $\mu\text{SR}$  and rf experiments. Recently, extreme multiband superconductivity was found in  $\text{PrOs}_4\text{Sb}_{12}$  from heat transport measurements by Seyfarth *et al.*<sup>8,9</sup> Their thermal conductivity and other data are explained by small and large gaps  $\Delta_s, \Delta_l$  on different sheets of the Fermi surface, together with different Fermi velocities  $v_{Fs}, v_{Fl}$  and coherence lengths  $\xi_{s,l} \approx \hbar v_{Fs,l}/\Delta_{s,l}$ . A crossover field  $H_{c2}^S$ , which corresponds to the overlap of the vortex core electronic structure due to the band with the small gap, is given by  $\Phi_0/2\pi\xi_s^2 \approx 10 \text{ mT}$ ,<sup>9</sup> which is of the order of the lower critical field  $H_{c1}$ . Microscopic calculations of the local DOS in a two band superconductor<sup>6</sup> suggest that the small gap will induce spatially extended QP states at low field. For  $H > H_{c2}^S$ , these loosely bound states overlap and become delocalized, with the dominant contribution to the DOS coming from the large gap band. In  $\text{PrOs}_4\text{Sb}_{12}$  this high-field region comes most of the vortex state; it is in this sense that  $\text{PrOs}_4\text{Sb}_{12}$  is an extreme multiband superconductor. Our TF- $\mu\text{SR}$  measurements were performed for applied field  $\mu_0 H = 10 \text{ mT} \approx H_{c2}^S$ . Then the small-gap

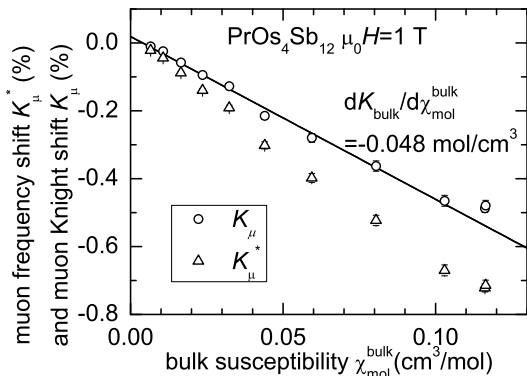


FIG. 5: Dependence of  $\mu^+$  frequency shift  $K_\mu^*$  and corrected  $\mu^+$  Knight shift  $K_\mu$  on bulk molar susceptibility  $\chi_{\text{mol}}^{\text{bulk}}$  in  $\text{PrOs}_4\text{Sb}_{12}$ , applied field  $\mu_0 H = 1 \text{ T}$ . The straight line  $K = K_{\text{bulk}}$  (see text) is a fit to the data in the region  $6.3 \text{ K} \leq T \leq 250 \text{ K}$ .

emu mole<sup>-1</sup> ( $T \gtrsim 6.3 \text{ K}$ ). This implies that at high temperatures the  $\mu^+$  shift samples the same electrons that produce the large temperature-dependent bulk susceptibility component. Such behavior is generally expected

states and their contributions to screening supercurrents are nearly uniform, the vortex-state field inhomogeneity is mainly due to large-gap supercurrents, and  $\lambda$  exhibits an activated temperature dependence if the large gap is nodeless. In contrast, the rf surface measurement was performed in the Meissner state. Both large- and small-gap Cooper pairs contribute to the superfluid density. Its temperature dependence is controlled by both small- and large-gap superfluid densities; the small-gap contribution dominates the temperature dependence at low temperatures. Then the temperature dependence of penetration depth from  $\mu$ SR is weaker than that in the Meissner state from rf measurements. This picture is qualitative and somewhat speculative; to our knowledge there is no theory yet for the temperature dependence of the vortex-state field distribution. It should also be noted that the TF- $\mu$ SR measurements give no information on the nodal structure of the small gap.

### B. Low-temperature Knight shift

In Fig. 5, a small deviation from the linear relation of the  $\mu^+$  Knight shift  $K_\mu$  vs bulk paramagnetic susceptibility  $\chi^{\text{bulk}}$  appears below 6.3 K in PrOs<sub>4</sub>Sb<sub>12</sub>. Kaplan, Schenck *et al.* have reported deviations from linear  $K_\mu$ - $\chi$  relations from TF- $\mu$ SR measurements of the  $\mu^+$  Knight shift in single crystals of PrNi<sub>5</sub><sup>29,30,31</sup> and PrIn<sub>3</sub>.<sup>32</sup> These were attributed to  $\mu^+$ -induced changes of the low-temperature susceptibility due to modification of the CEF of neighboring Pr<sup>3+</sup> ions. We argue that the  $\mu^+$ 's perturbing effect is small in PrOs<sub>4</sub>Sb<sub>12</sub> for the following reasons:

- The deviation of  $K_\mu(\chi)$  from linearity in PrOs<sub>4</sub>Sb<sub>12</sub> is very small. It might be due to other mechanisms, such as modification of the hyperfine interaction by thermal population of the CEF states.<sup>45</sup>
- The superconducting transition temperature measured by TF- $\mu$ SR is consistent with the bulk superconducting value (see Fig. 1), so that this signature of superconductivity is not affected by the  $\mu^+$  charge.
- Pr<sup>3+</sup> ions are considerably more dilute in PrOs<sub>4</sub>Sb<sub>12</sub> than in PrNi<sub>5</sub> or PrIn<sub>3</sub>. The experimental slope  $K_{\text{bulk}}$  vs  $\chi_{\text{mol}}$  in PrOs<sub>4</sub>Sb<sub>12</sub>,  $-4.8 \times 10^{-2}$  mol cm<sup>-3</sup>, is smaller than the corresponding values in PrNi<sub>5</sub> (Ref 29) and PrIn<sub>3</sub> (Ref 32) by more than an order of magnitude, indicating the dependence of Knight shift on the atomic susceptibility of Pr<sup>3+</sup> ions is weaker in PrOs<sub>4</sub>Sb<sub>12</sub>. In addition, the nearest-neighbor distance between  $\mu^+$  and Pr<sup>3+</sup> is about 2 Å longer in PrOs<sub>4</sub>Sb<sub>12</sub> than in PrNi<sub>5</sub> or PrIn<sub>3</sub>; thus for comparable screening lengths the  $\mu^+$  electric field at neighboring Pr<sup>3+</sup> sites is more completely screened by the conduction electrons.

- Schenck *et al.* concluded from ZF- $\mu$ SR studies<sup>46</sup> that the spin fluctuations of the Pr<sup>3+</sup> electronic moments in PrNi<sub>5</sub> are slowed down and exhibit quasistatic behavior at low temperatures. They suggested that this behavior is related to  $\mu^+$ -induced modification of the low temperature susceptibility of the neighboring Pr ions. We did not observe such large widths of the magnetic field distribution at low temperatures [see Fig. 4(c)]. Instead, our ZF- and LF- $\mu$ SR measurements suggest dynamic  $\mu^+$  relaxation solely by the <sup>141</sup>Pr nuclear spin system with an hyperfine-enhanced effective nuclear moment.<sup>47</sup>

We now discuss the small deviation from the linear relation that appears in Fig. 5 below 6.3 K. If we suppose this deviation is mainly due to the muon's perturbing effect, then this suggests that the  $\mu^+$  is monitoring a different susceptibility than the original bulk one, caused by local modification of the Pr<sup>3+</sup> CEF splitting. Hence, we can use the Knight shift data to find how much the Pr<sup>3+</sup> susceptibility is changed by the presence of the muon. To obtain a quantitative determination, we make the following assumptions as suggested by Schenck *et al.*:<sup>29,32</sup> (i) only the susceptibility of the two nearest Pr<sup>3+</sup> ions are affected by the muon, and (ii) only the two nearest Pr<sup>3+</sup> ions contribute to the contact interaction at the muon site. Based on these assumptions, with the principal axes of  $\chi$  chosen as the coordinate frame ( $\mathbf{x}, \mathbf{y}, \mathbf{z}$ ), the Knight shift with the external field in the  $i$  direction ( $i = x, y$  or  $z$ ) may be written as

$$K^i = (A_{\text{dip,NN}}^{ii} + A_{\text{con}})\chi_i^{\text{local}} + A_{\text{dip,(1-NN)}}^{ii}\chi^{\text{bulk}}. \quad (12)$$

Here  $\chi_i^{\text{local}}$  is the altered susceptibility of the two nearest Pr<sup>3+</sup> ions, and  $\chi^{\text{bulk}}$  is the unperturbed bulk Pr susceptibility. The subscript NN is used to signify that the sum in  $A_{\text{dip}}^{ii}$  only includes the two nearest Pr neighbors, whereas the subscript 1-NN indicates summation over all other Pr<sup>3+</sup> ions in the Lorentz sphere. For the most probable  $\mu^+$  site ( $\frac{1}{2}, 0, 0.15$ ),<sup>17</sup> the calculated values of  $A_{\text{dip}}$ ,  $A_{\text{dip,NN}}$ , and  $A_{\text{dip,1-NN}}$  are listed in Table II. We take  $A_{\text{con}}$  to be the slope of  $K_\mu$ - $\chi$  in Fig. 5, since the tensor  $A_{\text{dip}}$  is traceless and the sum of  $A_{\text{dip}}^{ii}$  vanishes as can be seen in Table II.

In order to obtain the values of  $\chi_i^{\text{local}}$ , we must modify  $\mathcal{H}_{\text{CEF}}$  to produce the required level changes. In the presence of a muon, the symmetry of the neighboring Pr<sup>3+</sup> ions is not the original cubic symmetry, but rather a very approximate tetragonal ( $C_{4v}$ ) symmetry. The general Hamiltonian describing this tetragonal symmetry is<sup>29,30</sup>

$$\mathcal{H}_{\text{CEF,tet}} = B_2^0 O_2^0 + B_4^0 O_4^0 + B_4^4 O_4^4 + B_6^0 O_6^0 + B_6^4 O_6^4, \quad (13)$$

which has five free parameters, compared to two in the original cubic Hamiltonian. In principle, the muon may modify the charge distribution around the Pr ions in every direction. However, if we only consider changes occurring along the Pr<sup>3+</sup>- $\mu^+$  axis for simplicity, it has been

TABLE II: Calculated values of coupling constants  $A_{\text{dip}}$ ,  $A_{\text{dip},1-\text{NN}}$ , and  $A_{\text{con}}$  (see text) in  $\text{PrOs}_4\text{Sb}_{12}$ .

$i$	$A_{\text{dip}}^{ii}$ (mol/cm <sup>3</sup> )	$A_{\text{dip},\text{NN}}^{ii}$ (mol/cm <sup>3</sup> )	$A_{\text{dip},1-\text{NN}}^{ii}$ (mol/cm <sup>3</sup> )	$A_{\text{con}}$ (mol/cm <sup>3</sup> )
$x$	$-4.64 \times 10^{-2}$	$-5.08 \times 10^{-2}$	$0.44 \times 10^{-2}$	
$y$	$2.51 \times 10^{-2}$	$2.18 \times 10^{-2}$	$0.33 \times 10^{-2}$	$4.8 \times 10^{-2}$
$z$	$2.01 \times 10^{-2}$	$2.18 \times 10^{-2}$	$-0.17 \times 10^{-2}$	

shown that the  $B_4^4$  and  $B_6^4$  remain at their cubic values.<sup>32</sup> This reduces the number of the free parameters from five to three. Hence, using Eq. (12), we can fit the muon Knight shift by choosing appropriate values of  $B_2^0$ ,  $B_4^0$ , and  $B_6^0$ . Our theoretical fits in  $\text{PrOs}_4\text{Sb}_{12}$  are shown in Fig. 6. The anisotropy is consistent with the new CEF and Eq. (12), decreases with increasing tem-

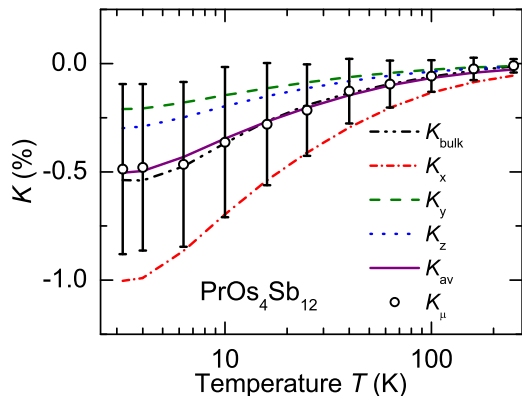


FIG. 6: Temperature dependence of muon Knight shift in  $\text{PrOs}_4\text{Sb}_{12}$ . Circles: muon Knight shift  $K_\mu$  from fig. 5. “Error bars:” Gaussian linewidth  $\delta K_\mu$  [Fig. 4(c)]. Dash-dot curve: calculated  $K_x$ . Dashed curve: calculated  $K_y$ . Dot curve: calculated  $K_z$ . Solid curve: average shift  $K_{\text{av}} = (K_x + K_y + K_z)/3$ . Dash-dot-dot curve:  $K_{\text{bulk}}$  from linear fit (Fig. 5), expected for no  $\mu^+$  perturbing effect.

perature, and is within the spread  $\delta K_\mu$  of muon shifts. The data are very well described by the average shift  $K_{\text{av}} = (K_x + K_y + K_z)/3$ , which is almost the same as  $K_{\text{bulk}}$  from Fig. 5 that assumes no  $\mu^+$  perturbing effect. The fitted CEF parameters are listed in Table I under the columns with heading  $C_{4v}$ . The changes in the parameters, which are very small and probably not statistically significant, give rise to a correspondingly small rearrangement of the local energy levels. A comparison of bulk and locally perturbed energy level scheme of  $\text{PrOs}_4\text{Sb}_{12}$  is shown in Fig. 7. We see that the change of splitting between the ground state and first excited state energies is only 1.8%, and conclude that the perturbing effect of the muon charge in  $\text{PrOs}_4\text{Sb}_{12}$  is negligibly small.

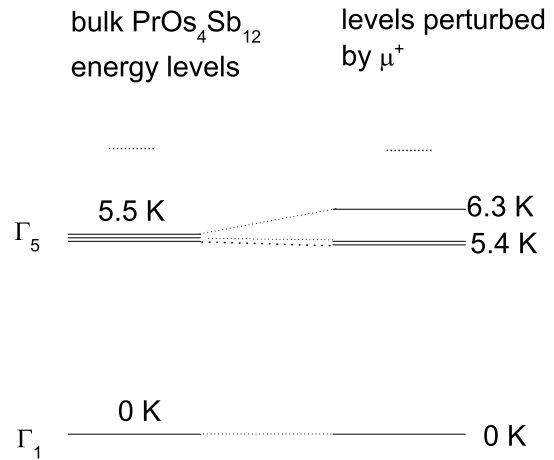


FIG. 7: Original bulk energy-level scheme of the Pr ions in  $\text{PrOs}_4\text{Sb}_{12}$ , compared to the local level scheme induced by  $\mu^+$ .

## V. CONCLUSIONS

In this paper we have presented TF- $\mu$ SR results in the first Pr-based heavy-fermion superconductor  $\text{PrOs}_4\text{Sb}_{12}$ . It is found experimentally that the effective penetration depth  $\lambda$  is temperature-independent in the vortex state for low temperatures, consistent with a nonzero gap for quasiparticle excitations. In contrast, rf inductive measurements suggest point nodes in the gap. This discrepancy can be resolved in a scenario based on the recent discovery of two-band superconductivity in  $\text{PrOs}_4\text{Sb}_{12}$ .

The temperature dependence of the normal-state  $\mu^+$  Knight shift in  $\text{PrOs}_4\text{Sb}_{12}$  reveals a linear scaling of the Knight shift with the bulk magnetic susceptibility at high temperatures. A very small deviation from the linear relation appears in  $\text{PrOs}_4\text{Sb}_{12}$  below 6.3 K. Such deviations have been explained by  $\mu^+$  induced modifications of the susceptibility of neighboring  $\text{Pr}^{3+}$  ions due to a change of the CEF splitting. Our data indicate, however, that this modification is very small in  $\text{PrOs}_4\text{Sb}_{12}$ . A model calculation based on CEF theory and the associated perturbed electronic energy levels confirms the smallness of the  $\mu^+$  perturbation effect. Therefore it is unlikely that the discrepancy between  $\mu$ SR and rf inductive measurements is caused by the muon charge.



### Acknowledgments

We are grateful for technical assistance from the TRIUMF Centre for Molecular and Materials Science during the experiments. This work was supported in part by the

U.S. NSF, grants 0422674 (Riverside), 0604015 (Los Angeles) and 0335173 (San Diego), by the Canadian NSERC and CIAR (Burnaby), and by the U.S. DOE (San Diego, Grant DE-FG-02-04ER46105). Work at Los Alamos was performed under the auspices of the U.S. DOE.

- 
- <sup>1</sup> H. Suhl, B. Matthias, and L. R. Walker, Phys. Rev. Lett. **3**, 552 (1959).
  - <sup>2</sup> R. S. Gonnelli, D. Daghero, G. A. Ummarino, V. A. Stepanov, J. Jun, S. M. Kazakov, and J. Karpinski, Phys. Rev. Lett. **89**, 247004 (2002).
  - <sup>3</sup> R. Cubitt, M. R. Eskildsen, C. D. Dewhurst, J. Jun, S. M. Kazakov, and J. Karpinski, Phys. Rev. Lett. **91**, 047002 (2003).
  - <sup>4</sup> S. Tsuda, T. Yokoya, Y. Takano, H. Kito, A. Matsushita, F. Yin, J. Itoh, H. Harima, and S. Shin, Phys. Rev. Lett. **91**, 127001 (2003).
  - <sup>5</sup> N. Nakai, M. Ichioka, and K. Machida, J. Phys. Soc. Jpn. **71**, 23 (2002).
  - <sup>6</sup> M. Ichioka, K. Machida, N. Nakai, and P. Miranović, Phys. Rev. B **70**, 144508 (2004).
  - <sup>7</sup> F. Gygi and Schlüter, Phys. Rev. B **43**, 7609 (1991).
  - <sup>8</sup> G. Seyfarth, J. P. Brison, M.-A. Méasson, J. Flouquet, K. Izawa, Y. Matsuda, H. Sugawara, and H. Sato, Phys. Rev. Lett. **95**, 107004 (2005).
  - <sup>9</sup> G. Seyfarth, J. P. Brison, M.-A. Méasson, D. Braithwaite, G. Lapertot, and J. Flouquet, Phys. Rev. Lett. **97**, 236403 (2006).
  - <sup>10</sup> E. D. Bauer, N. A. Frederick, P.-C. Ho, V. S. Zapf, and M. B. Maple, Phys. Rev. B **65**, 100506(R) (2002).
  - <sup>11</sup> M. B. Maple, P.-C. Ho, V. S. Zapf, W. M. Yuhasz, N. A. Frederick, and E. D. Bauer, Physica C **388-389**, 549 (2003).
  - <sup>12</sup> K. Takegahara, H. Harima, and A. Yanase, J. Phys. Soc. Jpn. **70**, 1190 (2001).
  - <sup>13</sup> M. B. Maple, P.-C. Ho, V. S. Zapf, N. A. Frederick, E. D. Bauer, W. M. Yuhasz, F. M. Woodward, and J. W. Lynn, J. Phys. Soc. Jpn. **71**, Suppl., 23 (2002).
  - <sup>14</sup> Y. Aoki, T. Namiki, S. Ohsaki, S. R. Saha, H. Sugawara, and H. Sato, J. Phys. Soc. Jpn. **71**, 2098 (2002).
  - <sup>15</sup> M. Kohgi, K. Iwasa, M. Nakajima, N. Metoki, S. Araki, N. Bernhoeft, J.-M. Mignot, A. Gukasov, H. Sato, Y. Aoki, and H. Sugawara, J. Phys. Soc. Jpn. **72**, 1002 (2003).
  - <sup>16</sup> E. A. Goremychkin, R. Osborn, E. D. Bauer, M. B. Maple, N. A. Frederick, W. M. Yuhasz, F. M. Woodward, and J. W. Lynn, Phys. Rev. Lett. **93**, 157003 (2004).
  - <sup>17</sup> Y. Aoki, A. Tsuchiya, T. Kanayama, S. R. Saha, H. Sugawara, H. Sato, W. Higemoto, A. Koda, K. Ohishi, K. Nishiyama, and R. Kadono, Phys. Rev. Lett. **91**, 067003 (2003).
  - <sup>18</sup> E. E. M. Chia, M. B. Salamon, H. Sugawara, and H. Sato, Phys. Rev. Lett. **91**, 247003 (2003).
  - <sup>19</sup> K. Izawa, Y. Nakajima, J. Goryo, Y. Matsuda, S. Osaki, H. Sugawara, H. Sato, P. Thalmeier, and K. Maki, Phys. Rev. Lett. **90**, 117001 (2003).
  - <sup>20</sup> A. D. Huxley, M.-A. Méasson, K. Izawa, C. D. Dewhurst, R. Cubitt, B. Grenier, H. Sugawara, J. Flouquet, Y. Matsuda, and H. Sato, Phys. Rev. Lett. **93**, 187005 (2004).
  - <sup>21</sup> R. Vollmer, A. Faißt, C. Pfeiderer, H. v. Löhneysen, E. D. Bauer, P.-C. Ho, V. Zapf, and M. B. Maple, Phys. Rev. Lett. **90**, 057001 (2003).
  - <sup>22</sup> M.-A. Méasson, D. Braithwaite, J. Flouquet, G. Seyfarth, J. P. Brison, E. Lhotel, C. Paulsen, H. Sugawara, and H. Sato, Phys. Rev. B **70**, 064516 (2004).
  - <sup>23</sup> K. Grube, S. Drobnik, C. Pfeiderer, H. v. Löhneysen, E. D. Bauer, and M. B. Maple, Phys. Rev. B **73**, 104503 (2006).
  - <sup>24</sup> D. E. MacLaughlin, J. E. Sonier, R. H. Heffner, O. O. Bernal, B.-L. Young, M. S. Rose, G. D. Morris, E. D. Bauer, T. D. Do, and M. B. Maple, Phys. Rev. Lett. **89**, 157001 (2002).
  - <sup>25</sup> J. H. Brewer, in *Encyclopedia of Applied Physics*, edited by G. L. Trigg (VCH Publishers, New York, 1994), Vol. 11, p. 23.
  - <sup>26</sup> J. E. Sonier, J. H. Brewer, and R. F. Kiefl, Rev. Mod. Phys. **72**, 769 (2000).
  - <sup>27</sup> W. Higemoto, S. R. Saha, A. Koda, K. Ohishi, R. Kadono, Y. Aoki, H. Sugawara, and H. Sato, Phys. Rev. B **75**, 020510 (2007).
  - <sup>28</sup> D. E. MacLaughlin, L. Shu, R. H. Heffner, J. E. Sonier, F. D. Callaghan, G. D. Morris, O. O. Bernal, W. M. Yuhasz, N. A. Frederick, and M. B. Maple, Physica B **403**, 1132 (2008).
  - <sup>29</sup> R. Feyerherm, A. Amato, A. Grayevsky, F. N. Gygax, N. Kaplan, and A. Schenck, J. Alloys Compounds **231**, 164 (1995).
  - <sup>30</sup> R. Feyerherm, A. Amato, A. Grayevsky, F. N. Gygax, N. Kaplan, and A. Schenck, Z. Phys. B, Condens. Matter. **99**, 3 (1995).
  - <sup>31</sup> R. Feyerherm, A. Amato, F. N. Gygax, A. Schenck, U. Zimmermann, A. Grayevsky, and N. Kaplan, Hyperfine Interact. **85**, 329 (1994).
  - <sup>32</sup> T. Tashma, A. Amato, A. Grayevsky, F. N. Gygax, M. Pinkpank, A. Schenck, and N. Kaplan, Phys. Rev. B **56**, 9397 (1997).
  - <sup>33</sup> E. H. Brandt, Phys. Rev. B **37**, 2349 (1988).
  - <sup>34</sup> L. Shu, D. E. MacLaughlin, R. H. Heffner, F. D. Callaghan, J. E. Sonier, G. D. Morris, O. O. Bernal, A. Bosse, J. E. Anderson, W. M. Yuhasz, N. A. Frederick, and M. B. Maple, Physica B **374-375**, 247 (2006).
  - <sup>35</sup> A. Amato, Rev. Mod. Phys. **69**, 1119 (1997).
  - <sup>36</sup> A. Schenck, in *Muon Spin Rotation Spectroscopy*, edited by E. W. J. Mitchell (Adam Hilger Ltd, Bristol, 1985).
  - <sup>37</sup> K. R. Lea, M. J. M. Leask, and W. P. Wolf, J. Phys. Chem. Solids **23**, 1381 (1962).
  - <sup>38</sup> T. Murao and T. Matsubara, Prog. Theor. Phys. **18**, 215 (1957).
  - <sup>39</sup> C. Niedermayer, C. Bernhard, T. Holden, R. K. Kremer, and K. Ahn, Phys. Rev. B **65**, 094512 (2002).
  - <sup>40</sup> R. Kadono, J. Phys. Condens. Matter **16**, S4421 (2004).
  - <sup>41</sup> T. Tayama, T. Sakakibara, H. Sugawara, Y. Aoki, and H. Sato, J. Phys. Soc. Jpn. **72**, 1516 (2003).
  - <sup>42</sup> A. Schenck, N. K. Sato, G. Solt, D. Andreica, F. N. Gygax, M. Pinkpank, and A. Amato, Eur. Phys. J. B **13**, 245 (2000).

- <sup>43</sup> P. G. Akishin and I. A. Gaganov, *J. Magn. Mag. Mat.* **110**, 175 (1992).
- <sup>44</sup> G. Carter, L. H. Bennet, and D. J. Kaham, *Prog. Mater. Sci.* **20**, 1 (1977).
- <sup>45</sup> D. E. MacLaughlin, O. Peña, and M. Lysak, *Phys. Rev. B* **23**, 1039 (1981).
- <sup>46</sup> N. Kaplan, A. Grayevsky, D. Shaltiel, S. Barth, P. Birrer, F. N. Gygax, B. Hitti, E. Lippelt, A. Schenck, and M. Weber, *Hyperfine Interact.* **85**, 271 (1994).
- <sup>47</sup> L. Shu, D. E. MacLaughlin, Y. Aoki, Y. Tunashima, Y. Yonezawa, S. Sanada, D. Kikuchi, H. Sato, R. H. Heffner, W. Higemoto, K. Ohishi, T. U. Ito, O. O. Bernal, A. D. Hillier, R. Kadono, A. Koda, K. Ishida, H. Sugawara, N. A. Fredeerick, W. M. Yuhasz, T. A. Sayles, T. Yangisawa, and M. B. Maple, *Phys. Rev. B* **76**, 014527 (2007).